Channel Interference in a Quasiballistic Aharonov-Bohm Experiment

G. Cernicchiaro,[1,4] T. Martin,[2,5] K. Hasselbach,[1] D. Mailly,[3] and A. Benoit[1]
[1]*CRTBT-CNRS, 25 av. des Martyrs, 38042 Grenoble, France*
[2]*CPT-Université d'Aix-Marseille II, Case 907, 13288 Marseille, France**
[3]*LMM-CNRS, 196 av. H. Ravera, 92220 Bagneux, France*
[4]*CBPF-CNPq, 150 av. Xavier Sigaud, 22000 Rio de Janeiro, Brazil*
[5]*Institut Laue–Langevin, B.P. 156x, 38042 Grenoble, France*
(Received 20 December 1996)

New experiments are presented on the transmission of electron waves through a two-dimensional electron gas ring with a gate on top of one of the branches. Magnetoconductance oscillations are observed, and the phase of the Aharonov-Bohm signal alternates between 0 and π as the gate voltage is scanned. A Fourier transform of the data reveals a dominant period in the voltage, interpreted as the energy spacing between successive transverse modes. A theoretical model including random phase shifts between successive modes reproduces the essential features of the experiment. [S0031-9007(97)03531-X]

PACS numbers: 73.40.–c

The Aharonov-Bohm (AB) effect has proven to be an invaluable tool for quantifying interference phenomena in mesoscopic physics. Early experiments on long metal cylinders [1] revealed that an electron accumulates a phase $\int \mathbf{A} \cdot d\mathbf{l}$ as it is scattered elastically by impurities while traveling around the loop: when the magnetic flux is varied, an oscillatory pattern with periodicity $h/2e$ results from the interference of an electron wave with its time reversed path [2]. Experiments on gold loops [3] confirmed that for normal metals which are laterally confined, the expected periodicity [4] is that of the *single* flux quantum $\phi_0 = h/e$. The amplitude of the magnetoresistance background can be understood within the framework of universal conductance fluctuations (UCF) [5]. The two-dimensional electron gas (2DEG) formed at the heterojunction between two semiconductors is used for experiments in the ballistic transport regime. Recently, oscillations associated with the modulation of the electron wavelength under the gate were observed in two experiments on gated rings in the diffusive [6] and the ballistic [7] regimes.

In the present Letter, results on a new AB transport measurement in the ballistic regime are reported. The number of lateral channels in one branch of the ring is adjusted by means of an electrostatic gate. Unlike previously, data are analyzed over the *whole* significant voltage range: from zero voltage to full depletion. A periodic pattern appears when the number of modes is modulated using the gate. Phase shifting and period halving in the AB pattern is monitored as the confinement is varied. The essential features of the data are interpreted using the scattering formulation of quantum transport [4]. The inclusion of disorder is necessary to explain the alternation of AB phases.

The 2D electron gas was created at the interface of a GaAlAs/GaAs heterojunction. A single loop device [8] of width 1.2 μm with inner diameter 4 μm connected to measurement leads was fabricated lithographically [Fig. 1(a)]. In this etched structure, the width of the wire constituting the ring is further reduced by a depletion of 0.27 μm at each edge. The 2DEG had a mobility of 1.14×10^6 cm^2/V s and an electron density of $n_s = 3.6 \times 10^{11}$ cm^{-2}. The coherence length $l_\phi > 20$ μm and the mean free path $l_e = 11,3$ μm indicate the ballistic regime. A metallic gate was deposited over one branch of the ring (the "upper" branch) allowing a controlled depletion of the 2DEG underneath. The number of electron channels N in the wires defining the ring was estimated assuming parabolic confinement in the transverse direction. The width W of the channel roughly equals the ratio of the 1D to the 2D electron density [9]. For $W = 600$ nm, and a Fermi wave length $\lambda_F = 40$ nm, $N = (3\pi/4)W/\lambda_F \approx 30$ channels. The lateral dimensions of the wire are comparable to those of the conductance quantization experiments [10], where the number of transmitted channels was shown to scale linearly with the depletion voltage.

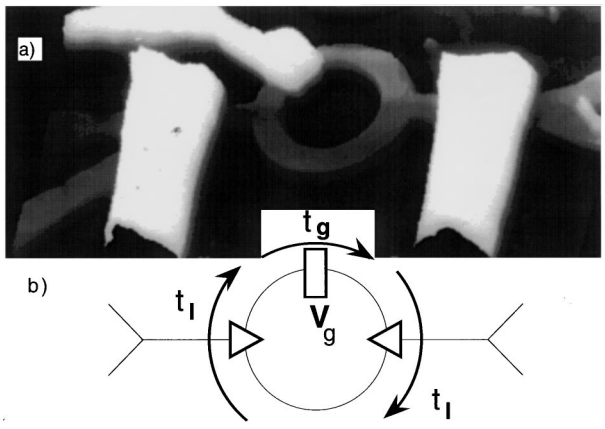

FIG. 1. (a) Atomic force microscope image: detail of a sample with the gate (white regions) over the upper branch and the gates for the leads. (b) A schematic diagram of the ring, beam splitters (triangles), and gate (see text).

The conductance was determined using standard synchronous detection measurements. A low-frequency ac current of 10 nA was injected and measurements were taken at 15 mK. An external magnetic field variation of 1.2 mT was applied corresponding to 4 flux quanta in the mean radius of the ring. While lowering the gate voltage from 0 to -300 mV by 1 mV steps, the complete conductance pattern was measured over a period of 4 hours. Digital filtering routines were applied to reduce base-line variations due to UCFs.

In Fig. 2, a "landscape plot" shows that the periodicity of the AB signal survives until a voltage of about -250 mV where the electrons underneath the gate are completely depleted and the ring is effectively cut off. When both arms transmit, shaded and clear areas alternate in the vertical direction, indicating oscillatory behavior as a function of the gate voltage. Attention is focused on the alternating contrast and the phase reversals when the gate voltage is increased. The smoothly changing background is identified as a residue of the total UCF signal. The AB phase of the pattern takes only values close to 0 or π [11]. The symmetry of the conductance under field reversal is associated with the two-terminal nature [12] of this measurement, as the spacing between the pair of current and voltage terminals on each side of the ring is not small compared to l_ϕ.

In Fig. 3, a magnetoresistance trace (inset) is displayed for a ring with one (both) branch(es) conducting: $V_g = -300$ mV ($V_g = 0$); the oscillatory signal appears to be an even function of flux. The corresponding Fourier signal shows a dominant component at the single flux quantum h/e. Higher harmonics have a much reduced amplitude.

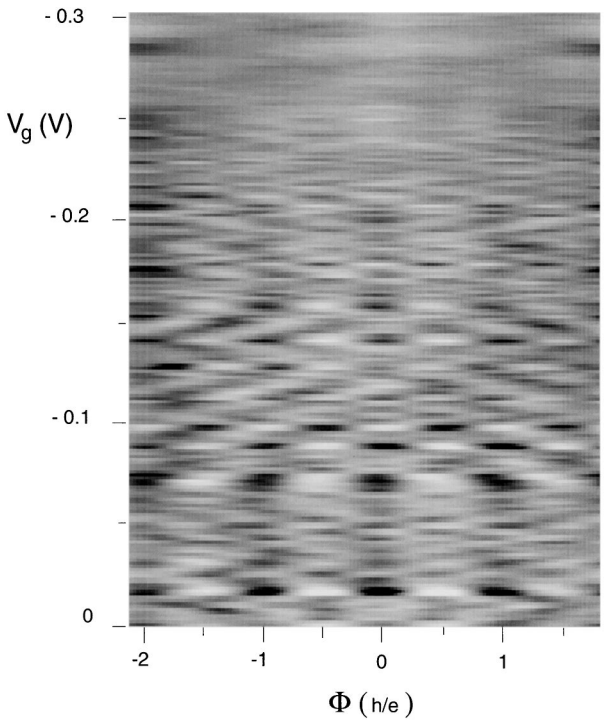

FIG. 2. AB component of the conductance, measured as a function of applied flux ϕ (horizontal axis) and gate voltage (vertical axis). Dark (clear) areas indicate minima (maxima) in the AB signal.

In Fig. 4, the modulus of the h/e Fourier component of the ring *resistance* is plotted for each value of V_g. The location of the transition between maxima and minima matches the position of the contrast changes in the conductance landscape (Fig. 2). While the location of the resistance peaks appears to be chaotic, a detailed analysis reveals a regular structure. Peaks of reduced magnitude persist between -200 mV and the depletion voltage.

Figure 5(a) shows the Fourier transform of the amplitude of the h/e harmonic, i.e., the data of Fig. 4 (computed over the range 0 to 256 mV). The three other spectra [Figs. 5(b)–5(d)] have a width 64 mV and an overlap of 14 mV between successive ranges. A dominant peak at 0.062 $(\mathrm{mV})^{-1}$ (arrow, center of figure) corresponding to a voltage period of 16 mV appears in each interval. The broadening of the peak in Figs. 5(b)–5(d) is associated first with the reduced voltage interval and second with the occurrence of other frequencies, attributed to the variation of the electron wavelength under the gate ([6,7]). Peaks located at 0.13 $(\mathrm{mV})^{-1}$ in Figs. 5(a), 5(c), and 5(d) correspond to higher harmonics. The persistence of the 16 mV oscillation in each interval signifies that it is linked to the opening or closing of transverse electron channels in the upper arm. The resulting magnetoresistance signal reflects how many channels in the upper branch contribute to the interference pattern.

The number of channels is extracted from the data by dividing the voltage range by the fundamental period. This number is a factor of 2 smaller than the geometrical estimate discussed above. However, the presence of a metallic gate induces changes in the electrical potential underneath, even at zero voltage (a positive voltage of a few hundred millivolts is necessary to open all channels [8]). The Fourier transforms of Figs. 5(b)–5(d) indicate that the peak at 0.062 $(\mathrm{mV})^{-1}$ carries less weight at

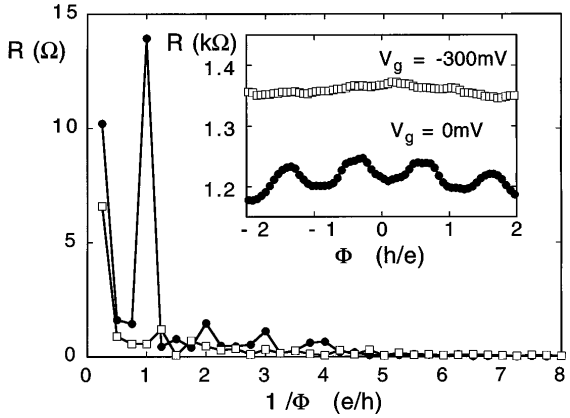

FIG. 3. Inset: Flux dependence of the sample resistance, for a closed ring (full dots) ($V_g = 0$ V) and a ring with one depleted branch (outline squares) ($V_g = -300$ mV) ring. Main figure: Fast Fourier transforms (FFT) of these signals after subtraction of an offset.

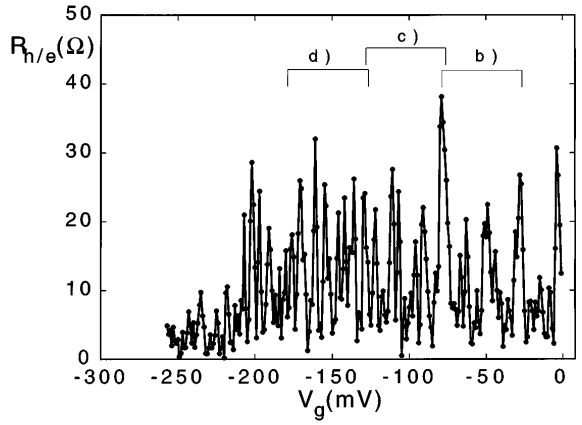

FIG. 4. Absolute value of the h/e Fourier component of the AB resistance as a function of gate voltage; brackets indicate subintervals used for the FFT in Figs. 5(b), 5(c), and 5(d).

higher voltages. This is consistent with the observation in Refs. [10] that the voltage spacing between successive steps in the conductance quantization ceased to be regular at high depletion.

Theoretically, the scattering approach for coherent transport [4] predicts a conductance,

$$G = 2\frac{e^2}{h}\sum_n |s_n|^2, \tag{1}$$

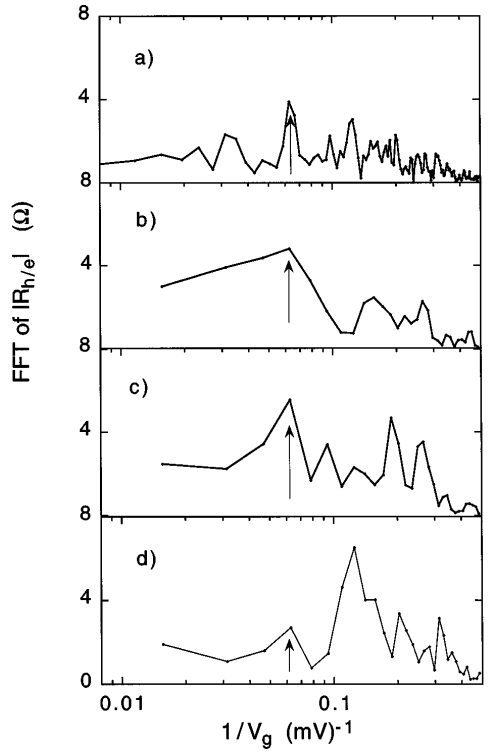

FIG. 5. The Fourier transforms of $R_{h/e}$ (Fig. 4) over the entire voltage range and three subintervals (see Fig. 4). The persistent peak at 0.062 $(\mathrm{mV})^{-1}$ corresponds to a voltage period of 16 mV.

where the sum is taken over the transverse modes, and the $|s_n|^2$ are the eigenvalues of the *transmission* matrix multiplied by its Hermitian conjugate. The splitting of the waves between the upper and lower branches (Fig. 1) is prescribed for each mode by a 3×3 scattering matrix [13]. No reflection is assumed in the lower branch. A scatterer with a quantized conductance [14] is located in the upper branch. A phase θ_n is added to the nth channel at the gate location. Electron waves are then recombined in the collecting lead, and the accumulated phase differences lead to an interference pattern. A simpler description excludes mixing between channels (backscattering). Nevertheless, the symmetry of the S matrix implicitly allows scattering between incoming and outgoing channels on each side. The transmission coefficient for electron waves in the nth channel is given by

$$s_n = -4\epsilon(\sqrt{1-2\epsilon}+1)^{-2}e^{i\pi\phi/\phi_0} \times [\,1 \quad 1\,][\mathbf{t}_l\mathbf{t}_g(n)\mathbf{t}_l e^{2i\pi\phi/\phi_0} - \mathbf{1}]^{-1}\begin{bmatrix} 1 \\ -1 \end{bmatrix}, \tag{2}$$

where ϵ specifies the connection of the current probes to the ring ($\epsilon_{\min} = 0$ for no coupling to the ring; $\epsilon_{\max} = 1/2$ for optimal coupling). $\mathbf{t}_l$ [$\mathbf{t}_g(n)$] is a 2×2 *transfer* matrix describing the beam splitters on each side (the gate in the upper branch); see Fig. 1(b). Note that the conductance of a perfectly symmetric, one-channel ring possesses sharp resonances at an integer number of ϕ_0. To mimic the inherent asymmetry of a fabricated ring, a small reflection (10%) was included in $\mathbf{t}_g(n)$. Calculations of the conductance landscape are shown for $N = 6$ channels. In Fig. 6(a) ($\theta_n = 0$ for all channels) the conductance pattern displays a staircase structure in the voltage direction which results from the progressive opening and closing of the channels in the upper branch. V_0 is the voltage necessary to suppress one channel. The AB signals of all channels are in phase.

A periodic variation of the phase shifts, $\theta_{n+1} - \theta_n = \pi$ (not shown, in Ref. [15]) leads to a halving of the AB period [16] for specific voltages. Peaks of reduced size arise at these voltages. The phase of the AB signal at zero flux is unperturbed.

A distinction is made between the global phase ϕ_{AB} of the AB signal and the channel shifts θ_n. Disorder is introduced by choosing random θ_n. Several configurations were tested, with the following conclusions: For a substantial depletion, peaks with a high conductance appear despite the reduced number of transmitting channels. ϕ_{AB} alternates between the two values 0 and π when the voltage is swept. In Fig. 6(b), $\theta_n = [0, \pi, \pi, 0, 0, \pi/2]$ were picked so as to highlight the pertinent features: The landscape contains an alternation of peaks shifted by π. A periodicity is observed in *both* the magnetic flux and the gate voltage. Finally, peak to valley variations of the conductance in Fig. 6(b) occur on a relatively small voltage scale [2 conductance steps of Fig. 6(a)].

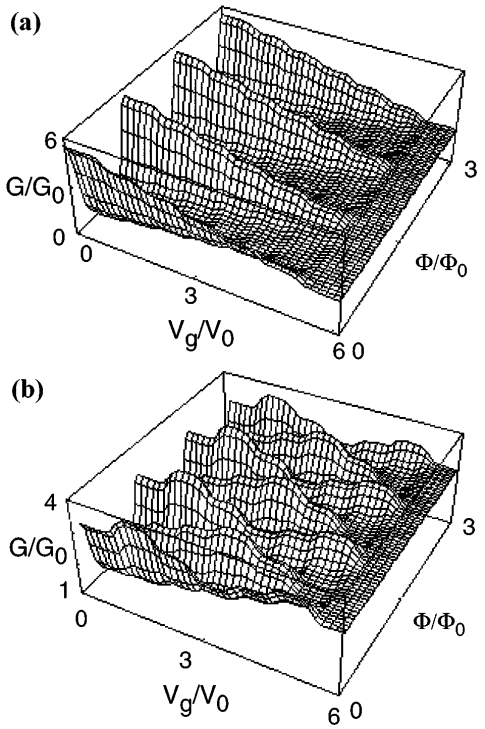

FIG. 6. (a) Calculated total transmission G ($G_0 = 2e^2/h$) through an Aharonov-Bohm ring with 6 modes, $\theta_n = 0$, as a function of flux and gate voltage. (b) Same calculation with $\theta_n = [0, \pi, \pi, 0, 0, \pi/2]$.

In conclusion, channel interference and conductance quantization explain the essential features of this Aharonov-Bohm experiment. When both arms are transmitting, the suppression of *one* single channel triggers fluctuations of the magnetoresistance which are comparable to the average signal, and may cause a shift of $\phi_{AB} = \pi$ of the pattern. Strikingly, the regular structure in the pattern persists from large depletion voltages, where few modes propagate in the upper branch (the typical conditions of Ref. [10]), to zero depletion voltages where most channels are transmitted. Our calculations reveal that random θ_n's must be included in the model to obtain the main features of the experiment, such as the sudden horizontal shifts ϕ_{AB} of the pattern and the large variations of the AB signal when the number of channels is reduced. Physically, this randomness originates from variations in path lengths suffered by different modes, from geometric scattering at the beam splitters, or from inhomogeneities in the confinement (impurities, etc.). Additional simulations [17], with $\theta_n = 0$ but channel mixing at the gate, lead to the same conclusions (pattern shifted by π) for specific configurations.

This work sheds further light on the issue of sudden phase changes in interference experiments. This geometry could possibly be used for the quantitative study of other scatterers (quantum billards, etc.) located on a branch of the ring: the analysis of the resulting AB pattern would then provide a way to quantify the role of disorder and the role of geometric scattering.

G. C. thanks L. Puech for useful discussions and acknowledges support by the CNPq, Brazil.

*Present address.

[1] D. Yu. Sharvin and Yu. V. Sharvin, Pis'ma Zh. Eksp. Teor. Fiz. **34**, 285 (1981) [JETP Lett. **34**, 272 (1981)].
[2] B. L. Altshuler, Pis'ma Zh. Eksp. Teor. Fiz. **33**, 101 (1981) [JETP Lett. **33**, 94 (1981)].
[3] R. A. Webb, S. Washburn, C. P. Umbach, and R. B. Laibowitz, Phys. Rev. Lett. **54**, 2692 (1985).
[4] M. Büttiker, Y. Imry, R. Landauer, and S. Pinhas, Phys. Rev. B **31**, 6207 (1985).
[5] P. A. Lee, A. D. Stone, and H. Fukuyama, Phys. Rev. B **35**, 1039 (1987); B. L. Altshuler, Pis'ma Zh. Eksp. Teor. Fiz. **41**, 530 (1985) [JETP Lett. **41**, 648 (1985)].
[6] S. Washburn, H. Schmid, D. P. Kern, and R. A. Webb, Phys. Rev. Lett. **59**, 791 (1987).
[7] A. Yacoby, U. Sivan, C. P. Umbach, and J. M. Hong, Phys. Rev. Lett. **66**, 1938 (1991); A. Yacoby *et al.*, Phys. Rev. Lett. **73**, 3149 (1994).
[8] D. Mailly, C. Chapelier, and A. Benoit, Phys. Rev. Lett. **70**, 2020 (1993).
[9] K. F. Berggren, G. Roos, and H. van Houten, Phys. Rev. B **37**, 10 118 (1988).
[10] B. J. van Wees *et al.*, Phys. Rev. Lett. **60**, 848 (1988); D. A. Wharam *et al.*, J. Phys. C **21**, L209 (1988).
[11] A. Yacoby, M. Heiblum, D. Mahalu, and H. Shtrikman, Phys. Rev. Lett. **74**, 4047 (1995).
[12] M. Büttiker, Phys. Rev. Lett. **57**, 1761 (1986); A. D. Benoit, S. Washburn, C. P. Umbach, R. B. Laibowitz, and R. A. Webb, *ibid.* **57**, 1765 (1986).
[13] M. Büttiker, Y. Imry, and M. Azbel, Phys. Rev. A **30**, 1982 (1983); Y. Gefen, Y. Imry, and M. Ya. Azbel, Phys. Rev. Lett. **52**, 129 (1984).
[14] M. Büttiker, Phys. Rev. B **41**, 7906 (1990); W. H. Miller, J. Chem. Phys. **48**, 1651 (1968).
[15] G. Cernicchiaro, Ph.D. thesis, Université Joseph Fourier, Grenoble, 1997.
[16] A. Yacoby, R. Schuster, and M. Heiblum, Phys. Rev. B **53**, 9583 (1996).
[17] G. Siffert *et al.* (unpublished).